

# NATIONAL AIR INTELLIGENCE CENTER



## THREE DIMENSIONAL CALCULATIONS OF ELECTRON BEAM PHASE SPACE DISTRIBUTION EFFECT

by

Weng Zili, Shi Yijin



Approved for public release:  
distribution unlimited

19960221 097

NAIC-ID(RS)T-0371-95

---

### HUMAN TRANSLATION

NAIC-ID(RS)T-0371-95

5 December 1995

MICROFICHE NR: 45 6000 750

THREE DIMENSIONAL CALCULATIONS OF ELECTRON  
BEAM PHASE SPACE DISTRIBUTION EFFECTS

By: Weng Zili, Shi Yijin

English pages: 24

Source: Qiangjiguang Yu Zizishu, Vol. 5, Nr. 2, May 1993;  
pp. 203-216

Country of origin: China

Translated by: SCITRAN

F33657-84-D-0165

Requester: NAIC/TATD/Dr. James Newton

Approved for public release: distribution unlimited.

THIS TRANSLATION IS A RENDITION OF THE ORIGINAL FOREIGN TEXT WITHOUT ANY ANALYTICAL OR EDITORIAL COMMENT STATEMENTS OR THEORIES ADVOCATED OR IMPLIED ARE THOSE OF THE SOURCE AND DO NOT NECESSARILY REFLECT THE POSITION OR OPINION OF THE NATIONAL AIR INTELLIGENCE CENTER.

PREPARED BY:

TRANSLATION SERVICES  
NATIONAL AIR INTELLIGENCE CENTER  
WPAFB, OHIO

NAIC-ID(RS)T-0371-95

---

Date 5 December 1995

---

# **GRAPHICS DISCLAIMER**

All figures, graphics, tables, equations, etc. merged into this translation were extracted from the best quality copy available.

Domestically, calculation results for rigorous three dimensional simulation programs have still not been published [1,2,3]. Due to FEL three dimensional simulation calculations being large in amount, it is necessary to think of designing a practically feasible three dimensional simulation program, and, in conjunction with this, maintain the rigor of three dimensional simulations, opting for the use of appropriate numerical value methods in order to guarantee that, under a presumption of adequate precision, shortening program operating time is the most key thing.

Going through a series of improvements, we designed the three dimensional program 3DFEL. Making use of this program, calculations were made in a relatively comprehensive way of electron beam quality and the influences of incidence mode on free electron laser operations. (1) Ideal Incidence. Comparisons are made with results that are already available to test 3DFEL program correctness and precision. (2) Different Emittences. Calculations point out that emittences are even more important indices than energy spreads. (3) Different Electron Phase Space Configurations. Only paying attention to electron beam emittences is not enough. Electron beam initial phase space configurations are also extremely important. They are not only capable of giving rise to very different equivalent energy spreads (capable of exceeding initial energy spreads). Moreover, they are also capable of influencing electron beam and light beam matching situations. Both of these have important influences on free electron laser operations. (4) Nonideal Incidence. We make calculations in connection with two relatively typical types of nonideal incidence--deviation incidence and oblique incidence--to explain nonideal incidence influences on FEL operations, thereby clarifying limiting conditions on beam flow delivery control.

## 2 BASIC EQUATIONS

3DFEL is aimed at long pulse single mode calculations which have not considered Slippage effects. Adoption is made of parabolic polar plane focused linear polarized undulators and linear polarized optical fields.

### Optical field equations

$$\frac{2ik_z}{L_w} \frac{\partial a_z}{\partial \tau} + \Delta_{\perp} a_z = -(S_z - iS_z) \quad (1)$$

$$S_z = \left\langle \frac{4\pi e a_w}{mc^3} J F_w \frac{\cos \psi}{\gamma} \right\rangle \quad (2)$$

/204

$$S_z = \left\langle \frac{4\pi e a_w}{mc^3} J F_w \frac{\sin \psi}{\gamma} \right\rangle \quad (3)$$

$$a_z = a_z + i a_z \quad (4)$$

### Electron longitudinal equations

$$\frac{d\gamma^2}{d\tau} = -2k_z a_w L_w F_w (a_z \sin \psi + a_z \cos \psi) \quad (5)$$

$$-\frac{d\cos \psi}{d\tau} = \delta k_w L_w \sin \psi \quad (6)$$

$$\frac{d\sin \psi}{d\tau} = \delta k_w L_w \cos \psi \quad (7)$$

$$\delta = 1 - \frac{k_z}{2\gamma^2 k_w} (1 + a_w^2 + (\gamma\beta_x)^2 + (\gamma\beta_y)^2) \quad (8)$$

### Electron transverse equations

$$\frac{d(\gamma\beta_x)}{d\tau} = -\frac{a_w^2 k_{wx}^2}{\gamma} L_w x \quad (9)$$

$$\frac{dx}{d\tau} = (\gamma\beta_x) L_w / \gamma \quad (10)$$

$$\frac{d(\gamma\beta_y)}{d\tau} = -\frac{a_w^2 k_{wy}^2}{\gamma} L_w y \quad (11)$$

$$\frac{dy}{d\tau} = (\gamma\beta_y) L_w / \gamma \quad (12)$$

In these

$$F_{\mu} = J_0(\mu) - J_1(\mu) \quad (13)$$

$$\mu = \frac{a_w^2}{2(1+a_w^2)} \quad (14)$$

$$k_w^2 = k_{wx}^2 + k_{wy}^2 \quad (15)$$

and

$$a_w(x, y, z) = a_w(z) (1 + k_{wx}^2 x^2 / 2 + k_{wy}^2 y^2 / 2) \quad (16)$$

$$a_x = - \frac{eE_x}{\sqrt{2} k_x mc^2} \quad (17)$$

$$a_w = - \frac{eB_w}{\sqrt{2} k_w mc^2} \quad (18)$$

$E_s$  and  $k_s$  are respectively electric field strengths and wave vectors associated with optical fields.  $B_w$  and  $k_w$  are respectively undulator magnetic field peak value strengths and wave vectors.  $\gamma$  is electron relativity theory factors.  $J$  is electron flow density.  $L_w$  is undulator length.  $\tau = ct/L_w$ ;  $J_{0,1}$  are respectively zero order and first order Bessel functions;  $\beta_x = v_x/c$ ;  $\beta_y = v_y/c$ ;  $\psi = (k_x + k_w)z - \omega t$ .

With regard to partial differential equations associated with optical fields, option is made for x and y direction alternate fully nonsalient normal solutions. Field boundary values are taken as 0. Optical field cross section dimensions are taken as  $10 w_0 \times 10 w_0$  ( $w_0$  is the optical waist radius). Divisions are into a 41x41 grid. The electron longitudinal equations make use of fourth order Runge-Kutta normal solutions. Electron transverse equations make use of first order difference solutions or opt for the use of adiabatic solutions. (With regard to program details, consider consulting reference [4]).

In order to facilitate comparisons with other programs, we opted for the use of parameters which were the same as the 5mm undulator in references [5] and [6]. Initial electron

distribution  $[\gamma, x, y, \gamma\beta_x, \gamma\beta_y, \sin\psi, \cos\psi]$  is given by Monte Carlo samplings.

As far as electron beams are concerned,  $\gamma \approx 100$ .  $\delta\gamma/\gamma \approx 1\%$  (energy spread).  $\epsilon_N = 0.14\text{cm}\cdot\text{rad}$  (normalized to 90% of emittance).  $I = 2\text{kA}$  (current strength). With regard to undulators,  $L_u = 500\text{cm}$ .  $\lambda_u = 8\text{cm}$ .  $B_u = 0.234\text{T}$ . In the case of optical beams,  $\lambda_s = 10.6\text{ microns}$  (wavelength).  $P_{in} = 10^6\text{ W}$  (input power).  $w_0 = 0.35\text{cm}$ . Sampling particle number  $N = 8192$ .

/205

Experience clearly shows that the initial distribution of  $\psi$  is very sensitive to influences associated with calculation results. Moreover, the disparities with regard to calculation results are very different for different samplings. This is caused due to inadequate particle numbers. Increasing particle numbers will increase calculation time. This is not a good method. We opted for the use of so called stable start methods [5]. 8192 sampling particles are divided into 8192/4 sets. Each set has 4 electrons. Values for the electrons in each set  $\gamma, x, y, \gamma\beta_x, \gamma\beta_y$  are given by sampling.  $\cos\psi$  and  $\sin\psi$  values are given by  $\psi = 0, \pi/2$ , and  $3\pi/2$ .

As far as electron beam radii  $r_e$  are concerned, the ones given by references [5] and [6] are 0.3cm. However, corresponding to emittance 0.14cm .rad, matching radii [7] are 0.444cm. As a result, in the calculations of Section III, in order to make comparisons with references [5] and [6], we adopt  $r_e = 0.3\text{cm}$ . In other calculations--if there is no special explanation--general adoption is made of  $r_e = 0.444\text{cm}$ .

### 3 PROGRAM RELIABILITY

In order to empirically verify program reliability, we carried out observations on the three points below.

1. Empty Field Evolution. Using Gaussian mode optical beams to act as input signals, what Fig.1(a) shows is the amplitude distribution graph in the  $x$  direction. Curves 1 and 2 are program simulation calculation results and analytical value comparisons (at undulator output location). The two curves are completely consistent with each other. In Fig.1(b), curves 1 and 2 are corresponding phase curves. They have some disparities at the edges. This is because--at the edges--we selected fixed 0 values as well as phase calculation  $\varphi = \text{tg}^{-1}(E_y/E_x)$ . Due to optical fields at the edges only being a few thousandths of values on axes and electron beams generally being located in the central portion, disparities associated with edges at this point have very small influences on our calculation results.

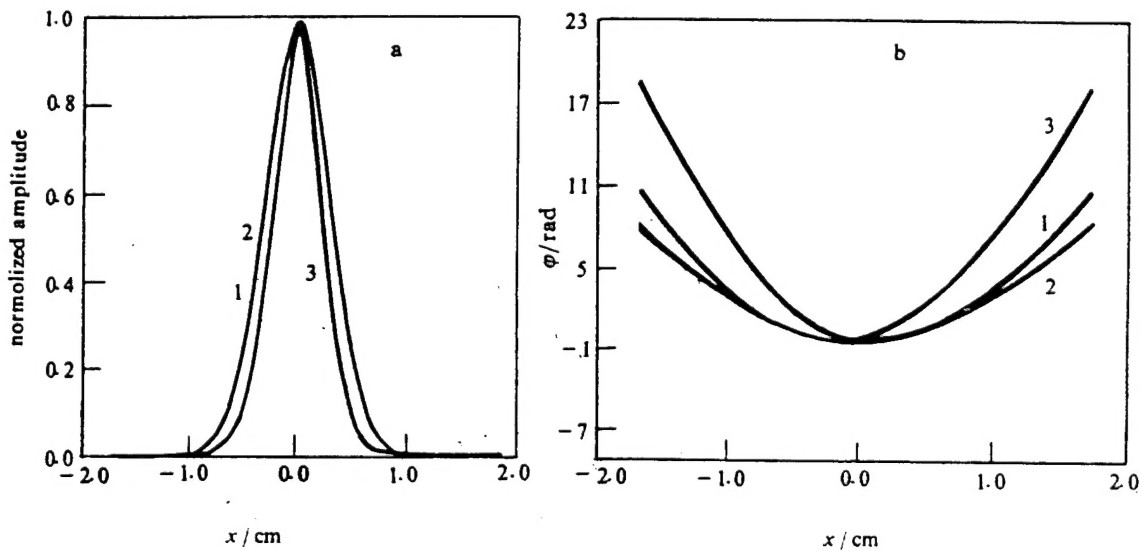


Fig. 1 (a) The comparison of the optical amplitude  $x$ -profile of the solution without  $e$ -beam. Curve 1 is numerical result; curve 2 the gaussian fundamental mode. For illumination the corresponding numerical result but with  $e$ -beam also is shown in Fig as curve 3. (b) the same but for phase.

2. In conditions where there is a source, we calculated electron power loses and optical power additions as shown in Fig.2. These two curves are completely consistent. The explanation for this is that the program in question is self-consistent.

3. We make comparisons between optical output powers when there is a source and other two dimensional rotary symmetry programs FRAD [6], MICFEL-DM, MICFEL-MFE [5]. Fig.3 shows that the results from our 3DFEL program are very close to FRED results.

/206

From the three points above, it can be seen that the 3DFEL program is reliable and possessed adequate precision.

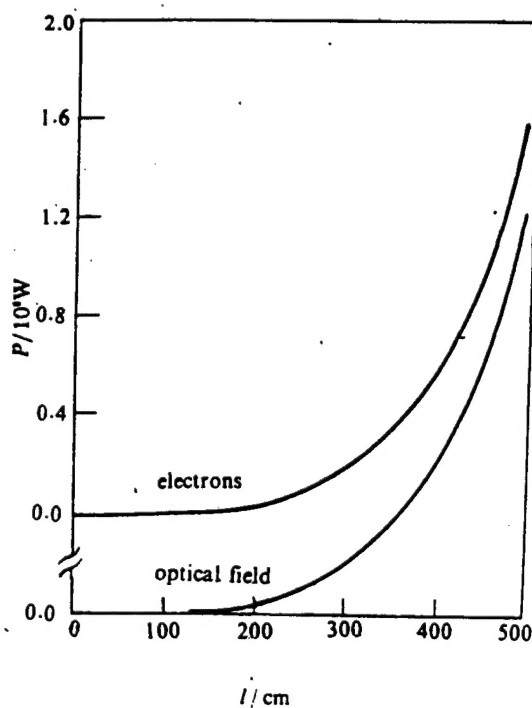


Fig.2 Comparison of the power growth of optical field and energy loss of electrons  
( $r_s = 0.3\text{cm}$ )

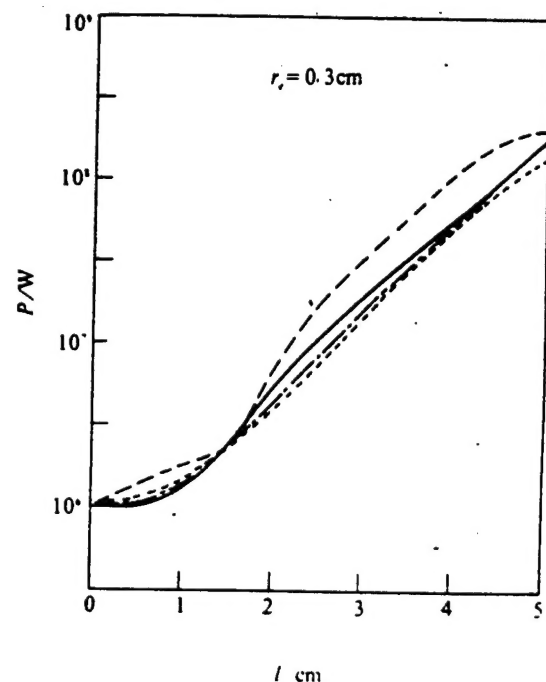


Fig.3 The evolution of optical power as a function of  $l$ , the undulator length. Solid line is the result of ours, dashed line and dotted line are for MICFEL<sup>DM</sup>, and dot - and - dash line for FRED<sup>M</sup> ( $r_s = 0.30\text{cm}$ )

#### 4 GAINS AND PHOTOCONDUCTANCE

Fig.4(a) is various types of different incident energies. It is laser power evolution curves in situations where electron beam radii  $r_e = 0.444\text{cm}$ . In the beginning phase, powers increase in a linear manner. After 100cm, there is exponential growth. Besides curve 1 showing saturation phenomena, the others still have not reached saturation. Fig.4(b) is corresponding evolution curves for each gain step. They clearly show that, in actuality, beyond 200cm is a zone of exponential growth. Gains begin a smooth slow decline. Moreover, before this, gains go through rapid phase aggregate increases. This is not consistent with small signal gain diagrams produced by second order aggregation mechanisms as generally understood. This means that, even if it is in a zone of linear increase, so long as electron captures occur, first order aggregation gains (that is, synchronous phase oscillation) given rise to by this still account for key contributions.

In Fig.4, the  $\gamma_0 = 102.0$  curve--in the initial phase--has larger gains than the others. However, later, its gains are smaller than the others. The explanation for this is that the initial phase is certainly not key with regard to final optical output powers. The key lies in electrons being forced into having mass kinetic capture situations as well as the quality of electron aggregation. This will directly influence optical gains in subsequent phases. The gains associated with this phase will present large differences, having very large influences on the magnitudes of final output powers.

As far as the calculations here are concerned, we adopted  $r_e = 0.444\text{cm}$ . Because, when emittance  $\epsilon_N = 0.14\text{cm. rad}$ , it is matching radius, electron beam envelope radii are, therefore,

maintained invariable [7]. As shown in Fig.6(a), this is advantageous to eliminating a number of complicated situations.

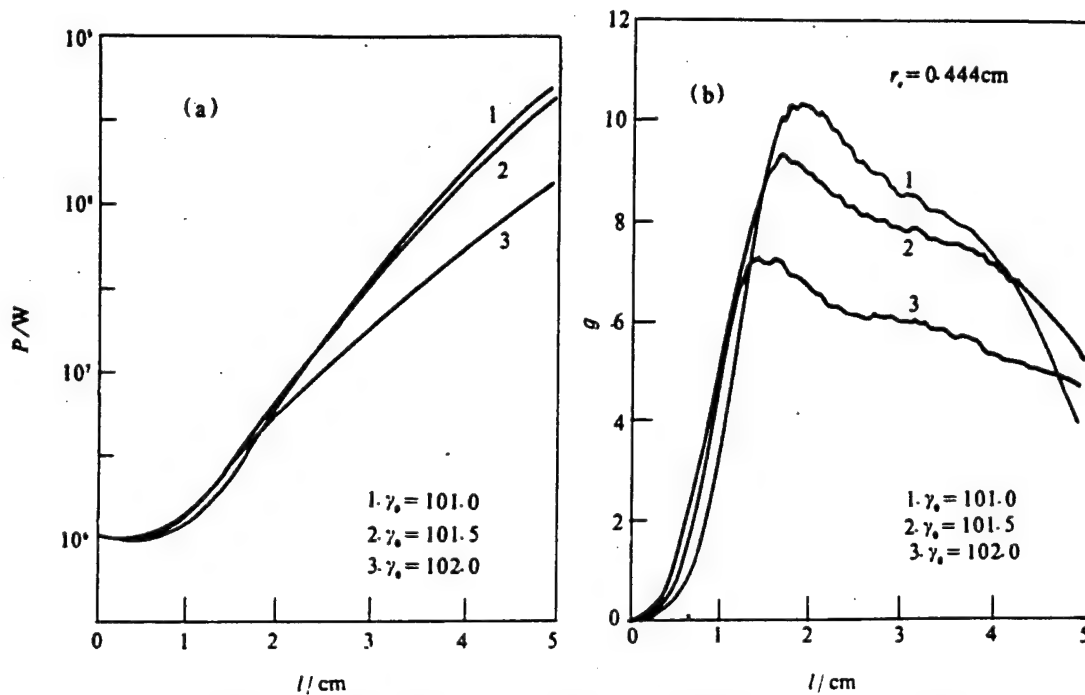


Fig. 4 (a) The evolution of optical power ( $r_e = 0.444\text{cm}$ ). (b) the gain per step as a function of  $l$ .

/207

Fig.5(a) and (b) are optical field amplitude and phase evolution process diagrams corresponding to curve 2 in Fig.4. In Fig.1(a) and (b), curve 3 is the corresponding undulator exit location distribution. For the purpose of making it stand out clearly, it is drawn together with empty field evolution results in order to be used in comparisons. Looking at optical field amplitude diagrams, exit location amplitude half heights and widths are smaller than entrance locations (in Fig.1(a), curve 3 compared to 1 and 2). What this shows is photoconductance phenomena. Looked at in terms of phase, at exit locations--making comparisons with empty field situations--phase curvature

radii are smaller than empty field situations (in Fig.1(b), curve 3 compared to 1 and 2). As a result, it seems that photoconductance is not then shown. The reason is that angles of emittance enlarge. Two types of photoconductance phenomena appear. Looking at amplitude diagrams, photoconductance gains bring with them the appearance of convergence on optical fields. Moreover, refractive photoconductance is true field convergence. However, looking at phase diagrams, appearances of refraction are defocused. As a result, in the case in question, we think that photoconductance phenomena certainly do not exist. From Fig.4, it can be seen that gain length (length associated with power increasing to be  $e$  fold the original) is approximately 87cm. It is  $1/4$  the Rayleigh length  $l_r = w_0^2 k / 2 \approx 360\text{cm}$ . Therefore, photoconductance gains cover up field diffraction effects [8], causing amplitude half heights and widths to be almost invariable after  $l=320\text{cm}$ . So long as optical beams enter free zones once they leave the undulator, they will scatter very fast.

## 5 INFLUENCE OF EMITTANCES ON OUTPUT POWERS

What Fig.7 shows is different emittances and optical output powers under conditions where electron radius  $r_e$  is adopted as a corresponding matching radius. Optical output powers follow along with emittance increases and decrease almost exponentially. With each one fold increase in emittance, power then drops an order of magnitude. As a result, emittance is the most important parameter influencing the size of output powers. With regard to this parameter, it is necessary--as conditions permit--to make it as small as possible. Below, we will make a further discussion of this in the area of equivalent energy spreads.

With regard to emittances giving rise to an equivalent energy spread, the factor in equation (8)

$$C = \frac{1}{2} a_w^2(z) (k_{wx}^2 x^2 + k_{wy}^2 y^2) + (\gamma\beta_x)^2 + (\gamma\beta_y)^2 \quad (19)$$

/208

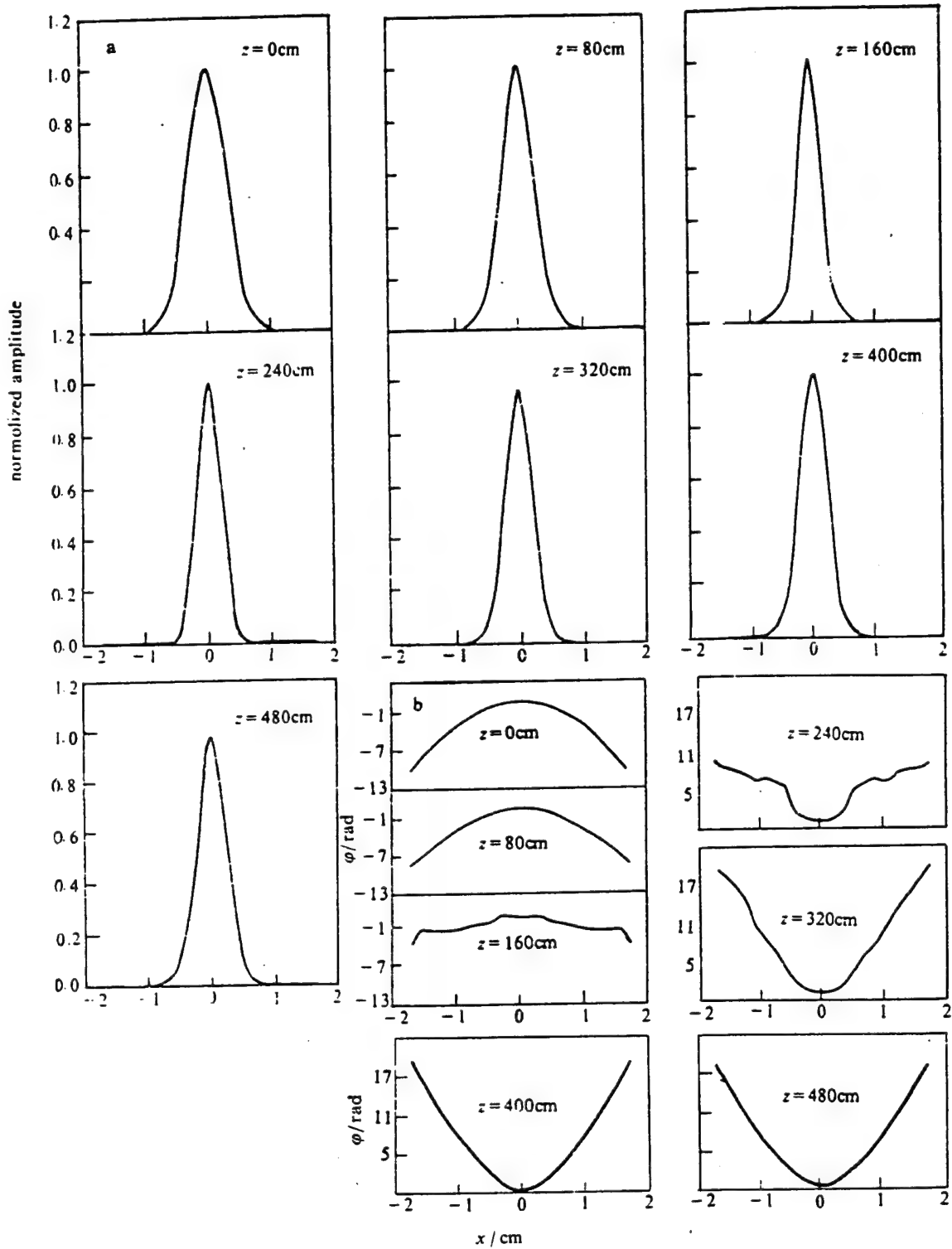


Fig. 5 (a) The evolution of the optical amplitude  $x$  - profile ( $r_e = 0.444\text{cm}$ ,  $\gamma_e = 101.5$ ).

(b) the same as (a) but for phase.

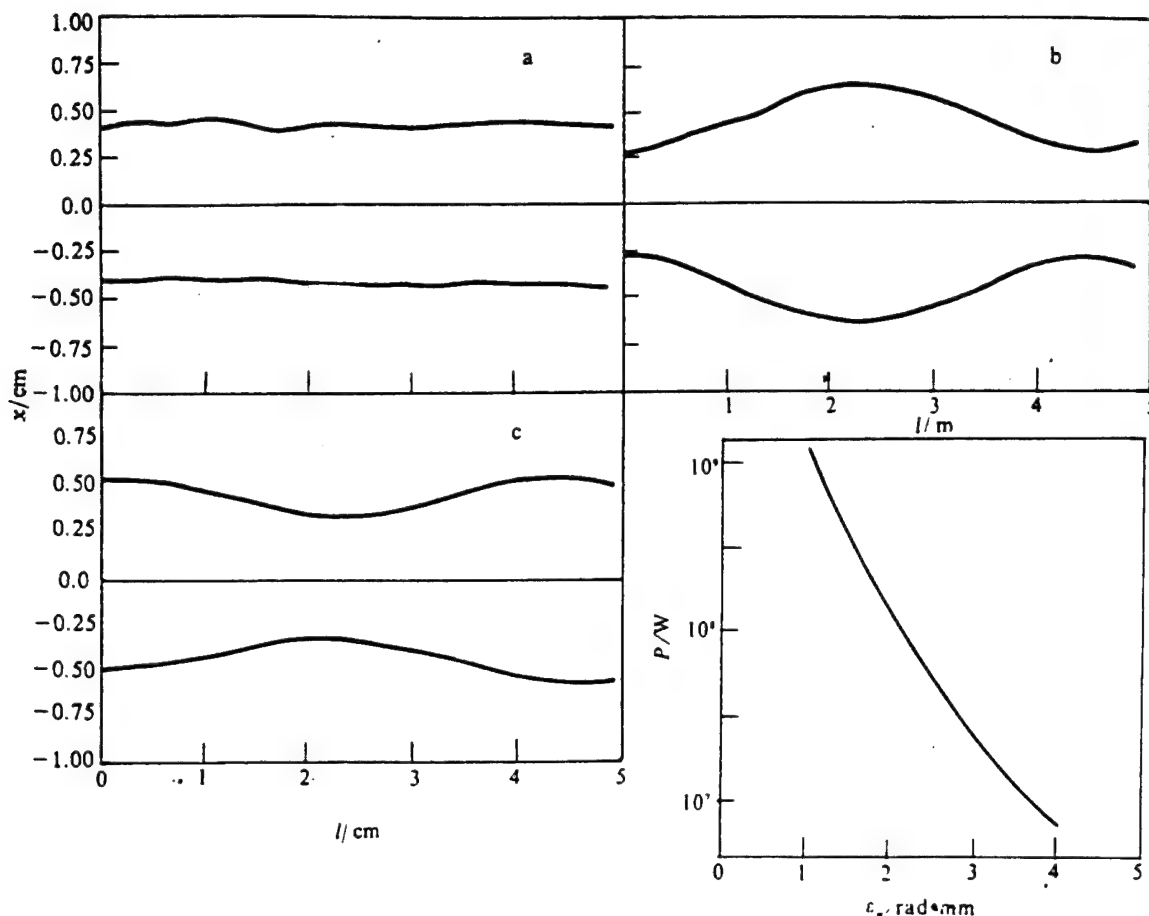


Fig. 6 The x envelop of e-beam with the waist of e-beam (a)  $r_e = 0.444 \text{ cm}$  (b)  $r_e = 0.30 \text{ cm}$  (c)  $r_e = 0.55 \text{ cm}$

Fig. 7 The output power as a function of the emittance of e-beam . (under the matched condition)

--speaking in terms of parabolic surface polar type undulators-- it is an adiabatic constant [6]. As a result, we introduce an equivalent amount of slippage

$$\delta_1 = 1 - \frac{k_z}{2\gamma_1^2 k_w} (1 + a_w^2(z)) \quad (20)$$

In the equation,  $\gamma_1 = \gamma + \Delta\gamma$ .

If  $\delta_1 = \delta$ , one gets

$$\Delta\gamma = - \frac{C\gamma}{2(1 + a_w^2)} \quad (21)$$

$\Delta\gamma$  is a negative number. With regard to different electrons--due to emittance--C values exist in a distribution, from 0-C<sub>max</sub>. Therefore,  $\Delta\gamma$  correspondingly has a distribution. As a result, even if the situation is one where incident electron beams have zero energy spread, the existence of emittance produces an additional equivalent energy spread. Assuming the  $\Delta\gamma$  distribution function is  $\rho_1(\Delta\gamma)$ , if the incident electron energy distribution is  $\rho_2(\gamma_2)$ , then, the equivalent incident energy distribution is a summation of  $\rho_1$  and  $\rho_2$ .

$$\rho(\gamma) = \int \rho_2(\gamma_2) \rho_1(\gamma - \gamma_2) d\gamma_2$$

/210

In order to calculate estimates of this additional equivalent energy spread  $\rho_1(\Delta\gamma)$ , we take c out of equation (8), maintaining the other equations invariable, that is, the effects given rise to by optical field amplitude increases and phases which are encountered for different transverse electron locations remain (This is another area of effects given rise to by emittance). In order to reveal equivalent energy spread effects that come with emittances, we calculated optical output powers for this situation with different initial energy spreads. In Fig.8(a), the solid line is corresponding calculation results. The broken lines are normal calculation values, that is, the output powers associated with curve 2 in Fig.4 (Its initial energy spread is 1%). The locations of intersections of solid and broken lines stand for energy spreads which are nothing else than a certain type of equivalent energy spread superposition mode given rise to by incident energy spreads and emittances. In order to make comparisons, we also calculated reference values for when initial equivalent energy spreads are zero, that is, the broken line with the dots in the Fig.'s. The energy spread values shown by intersection points between them and the solid lines are nothing else than the additional equivalent emittance energy spreads (approximately 1.25%). Fig.8(b) shows the same kind of results. However, this time, electron beams are in a

nonmatching state. Beam waist radii are 0.3cm. The additional equivalent energy spreads obtained from this are 2.05%. It should be pointed out that here broken lines and broken lines with dots are very close. This clearly shows that, when  $r_e = 0.30\text{cm}$ , emittance gives rise to an even larger additional energy spread, even to the point of the initial incident electron energy spread being a very small contribution to the total effective energy spread. In order to explain further, we assumed that energy spread superposition was close to square superposition.

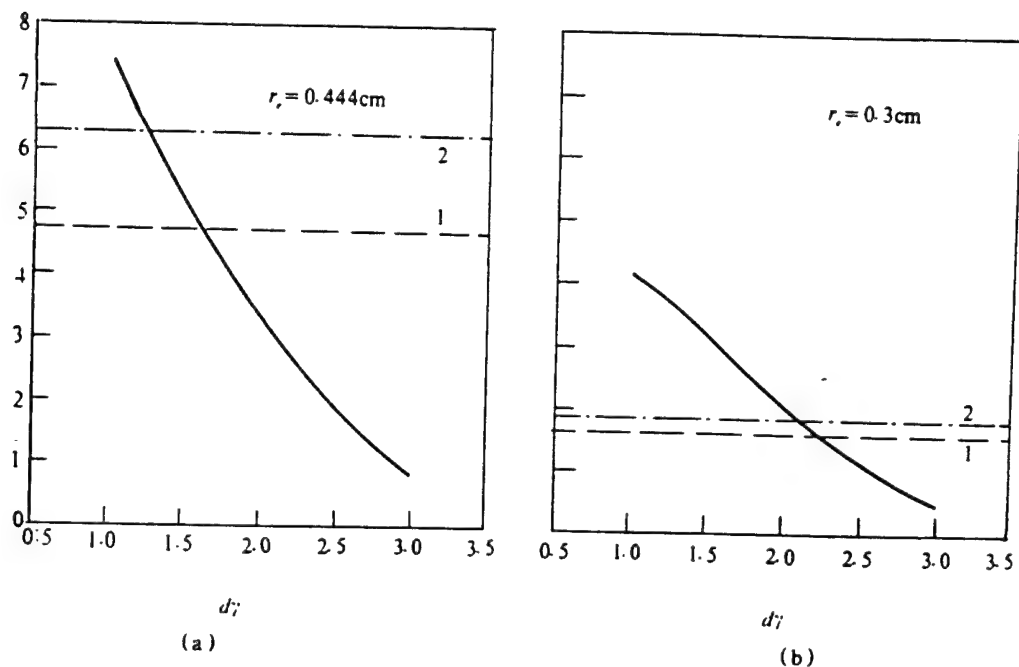


Fig. 8 The determination of the additional equivalent energy spread by the emittance.  
( $\varepsilon_v = 0.14\text{cm} \cdot \text{rad}$ ,  $r_e = 0.444\text{cm}$ ) (see the text)

As a result, one has  $[1.25^2 + 1.0^2]^{0.5} = 1.6(\%)$  ( $r_e = 0.444\text{cm}$ ),  $[2.05^2 + 1.0^2]^{0.5} = 2.3(\%)$  ( $r_e = 0.30\text{cm}$ ). 1.6 and 2.3 are very close to the equivalent energy spreads 1.65 and 2.2 given by intersection points of solid lines and broken lines in Fig. 8(a) and (b). The equivalent energy spreads given rise to by two types of matching methods are different.

It is generally thought that--with regard to emittance requirements--so long as  $e \sim \lambda_s$ , that will do. However, from this, we can see that a large additional equivalent energy spread given rise to because of emittance makes the role of initial incident electron energy spreads become unimportant. As a result, in our case, it is manifest that emittance is the number one factor to be considered. However, with regard to incident energy spread requirements, it is, by contrast, possible to see that the size of emittances is appropriately relaxed.

## 6 INFLUENCES OF DIFFERENT ELECTRON BEAM PHASE SPACE CONFIGURATIONS ON LASER OUTPUT POWERS

/211

Above, it was brought out that electron beam emittance plays two important roles with regard to laser outputs. One is equivalent energy spread. It makes resonance capable of producing diffusion and also causes changes to occur in mass kinetic force strengths. The second is giving rise to electron distribution in transverse directions as well as in envelope sizes, thereby influencing coupling with optical fields, that is, together with transverse distributions of strength and phase associated with optical fields, altering mass kinetic forces and synchronous phases. However, even if it is the same emittance, when initial electron phase space configurations are different, one will obtain different electron beam envelope configurations. Optical field coupling will also not be the same, then proceeding to cause light output powers to give rise to changes. In fact, it has already been put forward in Section I that additional equivalent energy spreads given rise to by different matching are capable of reaching one fold differences. Now, we are going to investigate this problem further.

## 6.1 Influences of Different Electron Beam Waist Radii on Output Powers

From electron transverse direction equations, it is possible to solve for electron matching radii (that is, electron envelope radii that are maintained invariable during movement processes) [7],  $r_e = (\frac{\sqrt{2} \epsilon_N}{a_w k_w})^{1/2}$ .

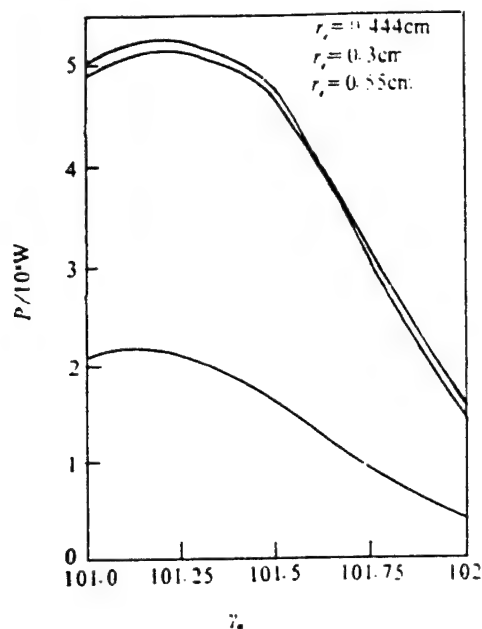


Fig.9 The output power as a function of the incident energy  $\gamma_0$  with different waist of e-beam. (the waists of e-beam are located on the entrance of undulator)

When  $\epsilon_N = 0.14 \text{ cm} \cdot \text{rad}$ ,  $r_e = 0.444 \text{ cm}$ . Respectively, we adopt  $r_e = 0.3, 0.444$ , and  $0.55 \text{ cm}$ . At the undulator entrance location, output powers were calculated when initial phase space was a right ellipse. As shown in Fig.9, optimum incident energies associated with different  $r_e$  are almost all  $\gamma_0 = 101.25$ . However, as far as  $r_e = 0.444$  and  $0.55 \text{ cm}$  are concerned, output powers are 2.5 times larger than  $r_e = 0.3 \text{ cm}$ .

Fig.6 is corresponding electron envelope diagrams. When  $r_e = 0.3 \text{ cm}$ , envelopes bulge up inside the undulator, electric field envelope superposition is small. However, when  $r_e = 0.444$  and  $0.55 \text{ cm}$ , electron envelope and optical field envelope overlap

is very good. Therefore, output powers are large. Electron beam envelope and optical field envelope superposition during the entire process is important. In our case, overlap associated with intermediate phases is even more important. This phase is the stage when optical powers increase the fastest. Incident electron beam radii are required to be between 0.444 - 0.55cm. Smaller than 0.444cm, and electron envelopes then bulge up in undulators. Larger than 0.55cm, envelopes inside undulators thin out some. However, the two ends are too large. This will not do either.

## 6.2 Influences of Different Electron Beam Waist Locations on Output powers

If one goes through movement systems, taking electron beam waists and translating them to the left (and maintaining emittance invariable), it makes electron beam waists fall into undulators (that is, entrance locations; electron beam phase space is an oblique ellipse). Adopting  $\gamma_0 = 101.5$ , we respectively calculated optical output powers when translation amounts are  $L = 0.2, 0.4, 0.6$ , and  $0.8 L_v$ . What Fig.10(a) shows is that, with regard to  $r_e = 0.3\text{cm}$ , when  $L=0.4L_v$ , output powers are maximum--almost twice when  $L=0.0L_v$ . Moreover, at this time, electron beam envelopes and optical field envelopes overlap together very well as shown in Fig.10(b).

As far as  $r_e = 0.444\text{cm}$  is concerned, due to electron beam envelope radii being maintained invariable, as a result, envelope translations have no influence on output powers.

## 7 NONIDEAL INCIDENCE

With regard to electron beams associated with undulators incident from transmission systems, the envelope center locus is not capable of completely overlapping with undulator magnetic

axes, with the appearance of deviation incidence and oblique incidence phenomena (We state that, in undulator entrance locations, electron beam incidence axes and magnetic axes are parallel. However, if they are not superimposed, there is deviation incidence. It is stipulated that the two axes intersect at entrance locations, however, if they are not parallel, there will be oblique incidence). At this time, optical output powers will then give rise to changes. What we need to understand is to how great an extent nonideal incidence influences optical output powers and to how great an extent deviation incidence and oblique incidence are permissible. That is also nothing else than to say that, within this range, output powers will not change very greatly. In this way, we will then be able to provide rational solutions for output systems.

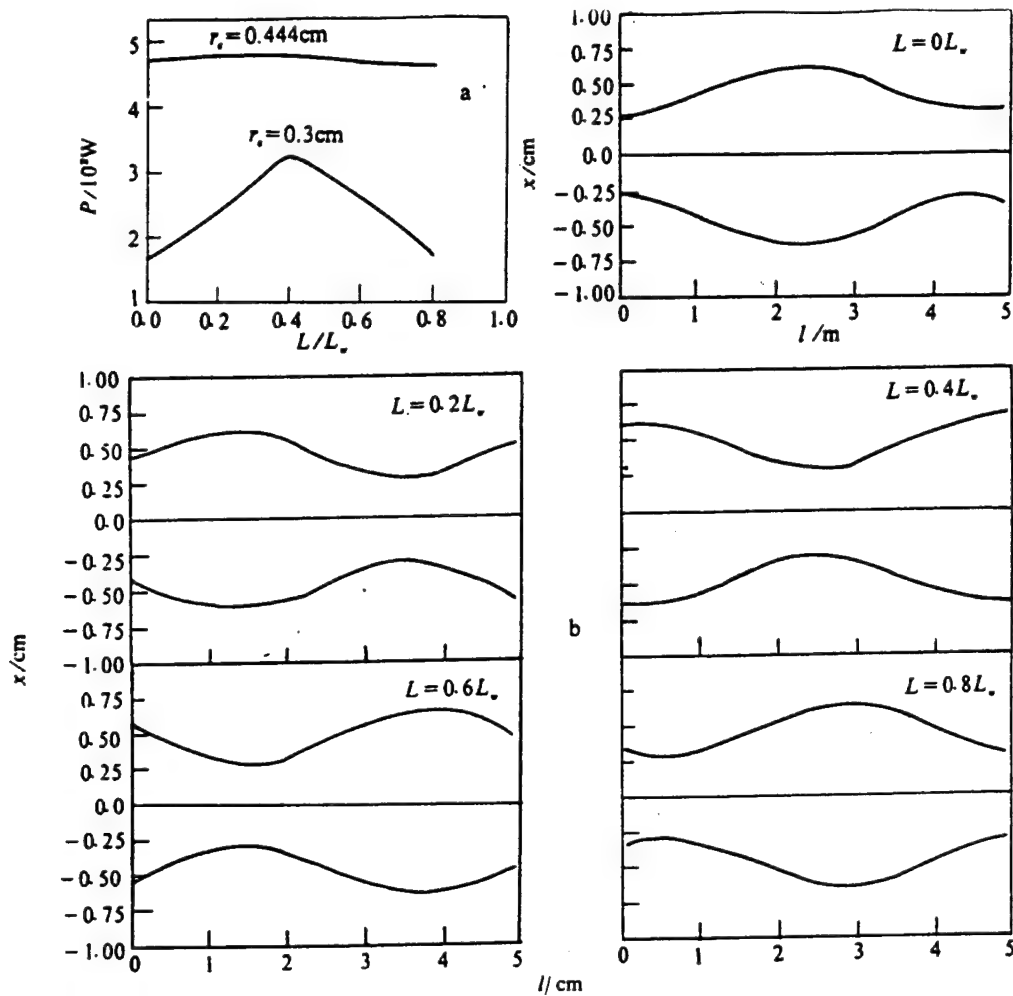


Fig. 10 (a) The output power as a function of  $\gamma_0$  with different locations of waist of e-beam.  
 (b) the corresponding envelopes of e-beam with  $r_0 = 0.30 \text{ cm}$ .

### 7.1 Deviation Incidence

We respectively take degrees of deviation incidence to be  $dx/r_0 = -0.3, -0.2, -0.1, 0.0, 0.1, 0.2, 0.3, 0.4, 0.6, 0.8$  and  $dy/r_0 = -0.3, -0.2, -0.1, 0.0, 0.1, 0.2, 0.3, 0.4, 0.6, 0.8$  and calculated the corresponding power changes (Fig.11). It is possible to see that x and y directions are equivalent positive and negative directions and are symmetrical. The explanation is that the program calculation results are stable and reliable.

When amounts of deflection are greater than  $0.4 r_0$ , output powers follow along with amounts of deviation and decline exponentially. As a result, it is necessary for amounts of deflection to be controlled within the  $0.4 r_0$  range.

Fig.12(a) and (b) are cross section diagrams of output optical field amplitudes and electron envelopes in the  $x$  direction when  $dx/r_e = 0.8$ . Although electron beams are deviation incident, because of the matching radii adopted, however, electron beam envelope radii are, therefore, almost invariable. However, electron beams give rise to distortion.

From amplitude diagrams ( $x$  direction cross section diagrams), it is seen that, in the front half section, the center of gravity of the area under the curve is shifted toward the  $+x$  direction. This is due, in the forward half section, to electrons being primarily concentrated in the  $+x$  region (see envelope diagrams). In the case of the rear half section, the center of gravity gradually moves in the  $-x$  direction. At exit locations, the center of gravity is clearly shifted into the  $-x$  region. This is due to electrons rotating around the  $z$  axis during movements. In the bottom half section, electrons are primarily concentrated in the  $-x$  region. In the very initial phase, optical fields increase linearly. However, later on, the increases are exponential. Therefore, at output locations, the center of gravity finally appears in the  $-x$  region.

/213

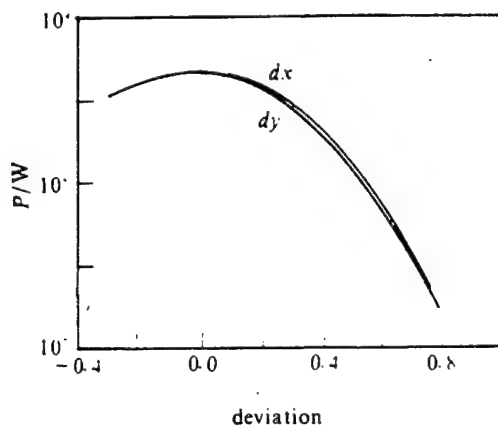


Fig. 11 The output power as a function of the incident deviation of  $e$ -beam in  $x, y$  directions ( $r_e = 0.444\text{cm}$ )

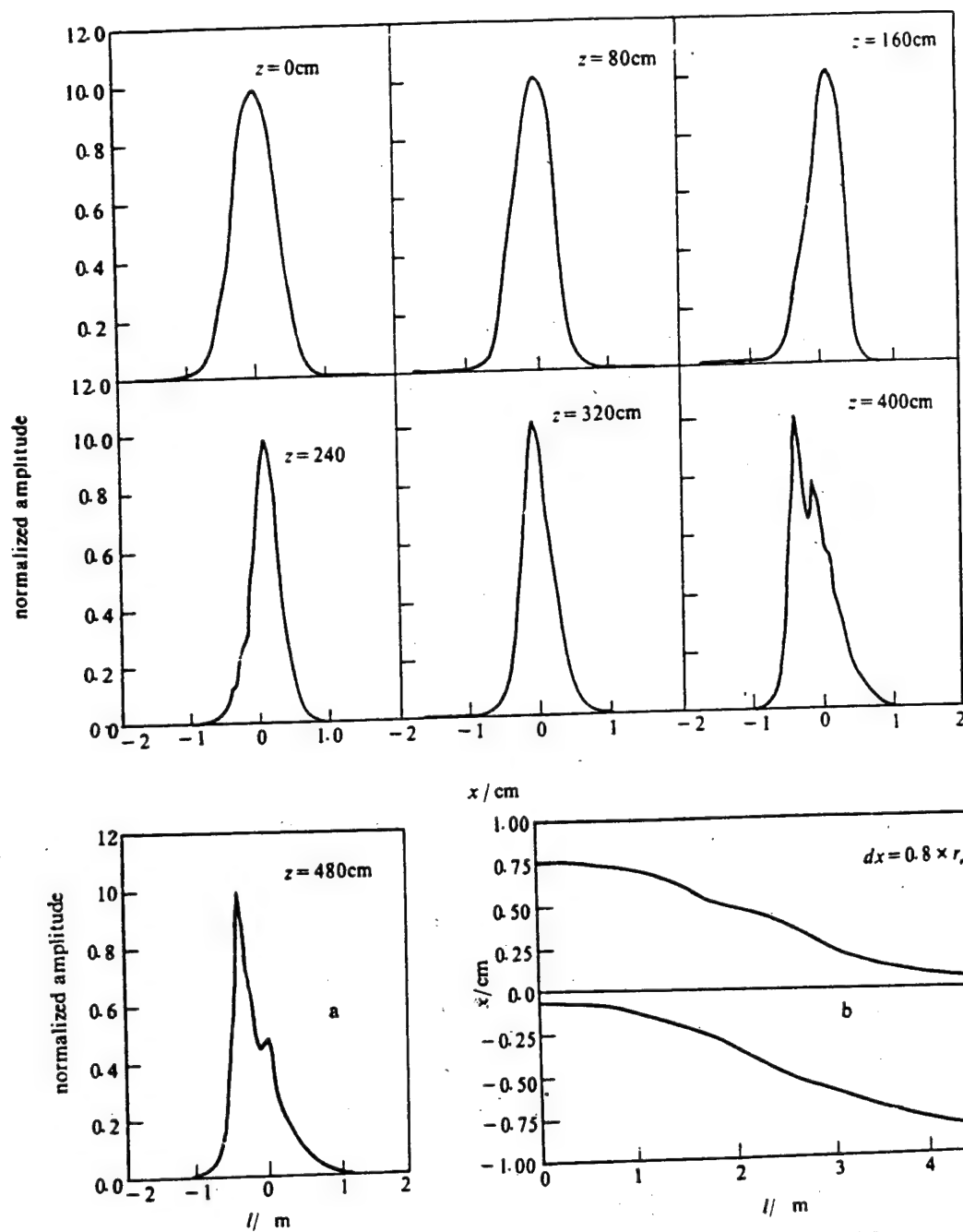


Fig. 12 (a) The evolution of optical amplitude  $x$ -profile with  $x$ -deviation  $0.8r$ ,  
(b) the same as in (a) but for phase

/214

Amplitude curves appear bent. The explanation for this is the appearance of higher order modes.

## 7.2 Oblique Incidence

We respectively took oblique incidence angles to be  $d\beta_x/\beta_{om} = -0.3, -0.2, -0.1, 0.0, 0.1, 0.2, 0.3, 0.4, 0.6, 0.8$  and  $d\beta_y/\beta_{om} = -0.3, -0.2, -0.1, 0.0, 0.1, 0.2, 0.3, 0.4, 0.6, 0.8$  and calculated corresponding power changes (Fig.13). In these

$$\beta_{om} = \epsilon_N / (\gamma r_e)$$

Results clearly show that, in the same way as deviation incidence, when oblique incidence is greater than 0.4, it gives rise to exponential decreases in optical output powers and the appearance of higher order modes. Fig.14 (a) and (b) are cross section diagrams in the x direction associated with optical field amplitudes and electron envelopes when  $d\beta_x/0.6\beta_{om}$ . The difference from deviation incidence lies in the centers of gravity of areas under amplitude curves being shifted into the + x region right through. This can be seen from electron beam envelope diagrams. Electrons are primarily shifted into the + x region in the entire phase. This is different from deviation incidence envelopes.

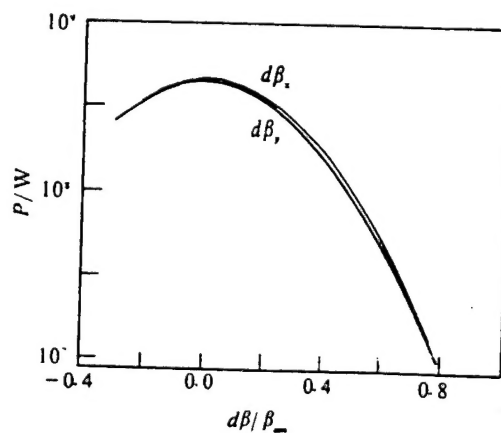


Fig. 13 The output power as a function of the incident obliqueness of e-beam in x, y directions. ( $r_e = 0.444\text{cm}$ )

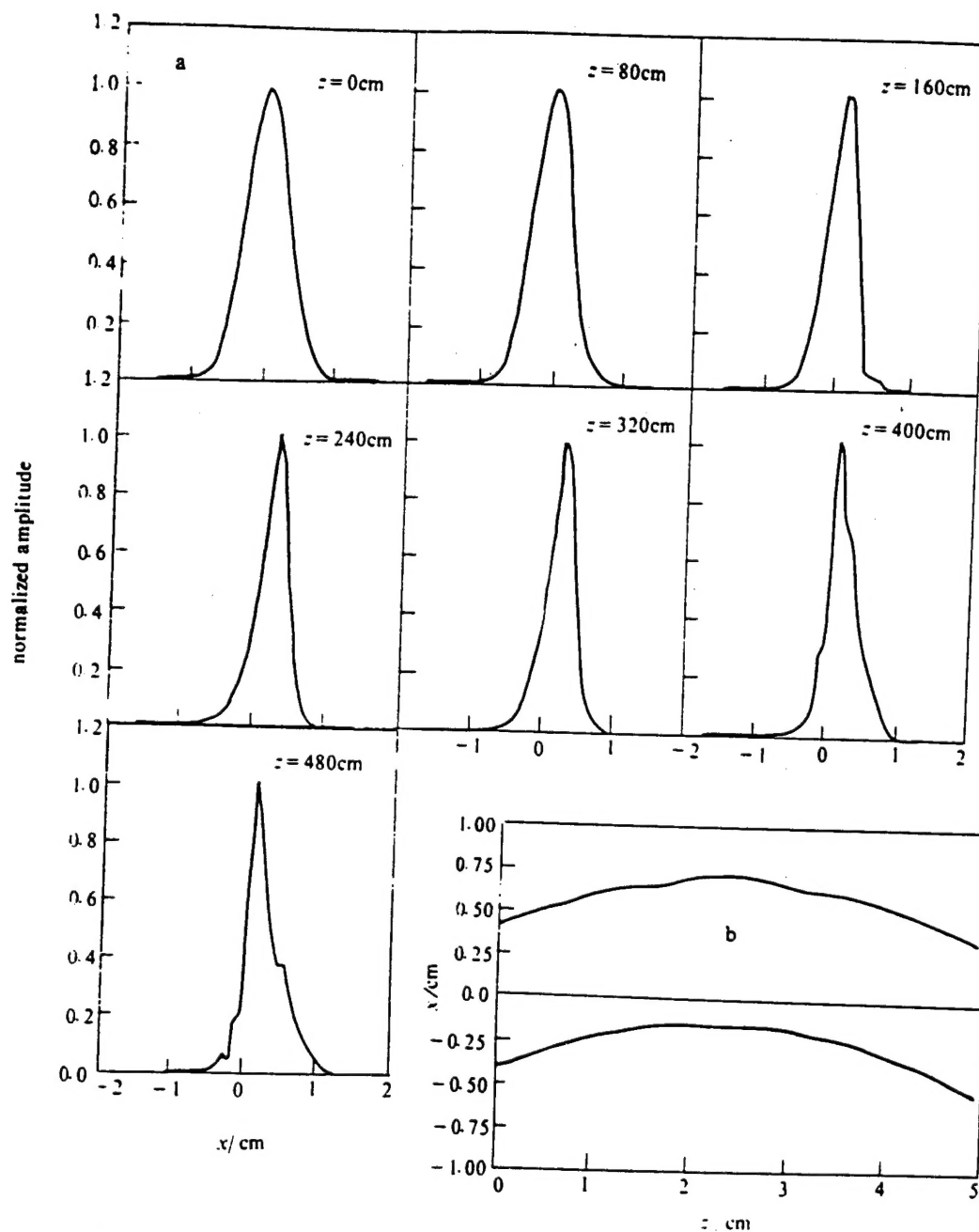


Fig. 14 (a) The evolution of optical amplitude  $x$ -profile with  $x$ -obliqueness  $0.6\beta_m$   
 (b) the same as in (a) but for phase

## 8 CONCLUSIONS

3DFEL program calculation results are reliable. We applied the program in question to some preliminary work. The primary conclusions were that emittance is an important parameter influencing free electron lasers. In our case, comparisons were made with energy spreads, and they seemed even more important. Moreover, it should be pointed out that, when there is a given emittance, initial electron beam phase space configurations are also an important parameter, requiring that adequate attention be paid to them. At the present time, operating the program in question requires 20 minutes of CPU time (386 microcomputer). Besides applying the program in question to further operations, in the next step, we will do three dimensional oscillator program design work.

## REFERENCES

- [1] 杨震华等. 强激光与粒子束, 1991, 3 (1): 115.
- [2] 杨震华等. 强激光与粒子束, 1991, 3 (2): 191.
- [3] 姜云卿等. 强激光与粒子束, 1991, 3 (2): 209.
- [4] 翁自立, 施义晋. 自由电子激光三维数值模拟程序. 计算物理, (待发表).
- [5] 王元璋等. 北京应用物理与计算数学研究所. FEL 第四次会议文集. 1989, 105.
- [6] Scharleman ET. *J Appl Phys*, 1985, 58: 2154.
- [7] 钱四海, 施义晋. FEL 数值计算中非旋转对称效应的二维模型. 强激光与粒子束, 1992, 4 (3): 349 ~ 356.
- [8] Moore GT. *Nucl Instru Method*, 1985, A239: 19.

DISTRIBUTION LIST

DISTRIBUTION DIRECT TO RECIPIENT

ORGANIZATION	MICROFICHE
B085 DIA/RTS-2FI	1
C509 BALL0C509 BALLISTIC RES LAB	1
C510 R&T LABS/AVEADCOM	1
C513 ARRADCOM	1
C535 AVRADCOM/TSARCOM	1
C539 TRASANA	1
Q592 FSTC	4
Q619 MSIC REDSTONE	1
Q008 NTIC	1
Q043 AFMIC-IS	1
E404 AEDC/DOF	1
E410 AFDIC/IN	1
E429 SD/IND	1
P005 DOE/ISA/DDI	1
1051 AFTT/LDE	1
PO90 NSA/CDB	1

Microfiche Nbr: FTD95C000750  
NAIC-ID(RS)T-0371-95